Catalysis Science & Technology

ROYAL SOCIETY OF CHEMISTRY

PAPER

View Article Online
View Journal | View Issue

Cite this: *Catal. Sci. Technol.*, 2025, **15**, 6196

Prospects of ethylene hydroformylation beyond Rh-based catalysts

Anjali Ganai and Pranab Sarkar *

Received 7th July 2025,
Accepted 27th August 2025

DOI: 10.1039/d5cy00818b

rsc.li/catalysis

Rh-based homogeneous catalysts with phosphine ligands have been typically used for catalysing hydroformylation reactions. Heterogenisation of Rh-based systems, however, introduces a side-reaction of ethylene hydrogenation. In order to enhance reaction selectivity, (1) immobilization of single atom catalysts onto supports like polymers, ZnO or CeO and (2) the use of promoters such as Co, Mo, V, and alkali metals have emerged as new strategies. However, all these studies involve the use of Rh, an expensive noble metal, as a catalyst. With the intention of designing a non-Rh-based catalyst with single site reactivity for ethylene hydroformylation, we have, for the first time, computationally investigated the role of UiO-68 decorated NHC-Cu(I)-H catalyst in catalysing the reaction. Mechanistic investigations suggest that it can selectively transform ethylene to propanal and can act as an alternative to the homogeneous Wilkinson's catalyst and also to various Rh-based heterogeneous catalysts.

1 Introduction

The hydroformylation reaction, also known as the oxo process, involves the production of aldehydes from alkenes using CO and H_2. In this process, a hydrogen and a formyl group is added to a carbon–carbon double bond with an atom economy of 100%.[1,2] The oxo process is typically catalysed in homogeneous systems using transition metal complexes of Co and Rh.[3–6] Rh-based catalysts with phosphine ligands are commonly used due to their high activity and selectivity. However, this commercial catalyst is beset by the immoderate cost of Rh and phosphine ligands. Additionally, loss of the noble metal is encountered during the catalyst separation process. Since the phosphine ligands are air and moisture sensitive, the search for phosphine-free heterogeneous catalysts has gained attention. However, the supported ligand-free metal catalysts suffer from low reaction selectivity; hydrogenation products are found to occur through a competing side reaction. Two methods have currently emerged in order to enhance reaction selectivity towards oxygenate products – (1) immobilizing single atom catalysts onto supports like polymers, ZnO or CeO[7–9] and (2) the use of promoters such as Co, Mo, V, alkali metals, *etc.*[10–13]

However, previous studies on hydroformylation reactions have used Rh-based catalysts in enhancing the reaction activity and selectivity;[14] none of them has focused on designing a Rh-free catalyst for the hydroformylation reaction.

Metal–organic frameworks (MOFs), composed of metal nodes and organic linkers, have now emerged as an effective platform for converting homogeneous systems into its heterogeneous analogues.[15] The porous structure, high surface area and tunability of the metal node or organic linkers make MOFs an attractive choice for catalysing various reactions. MOFs provide an added advantage of designing isolated active sites in the form of single atom catalysts *via* modification of organic linkers.[16–18]

With the intention of designing a Rh-free single atom catalyst for ethylene hydroformylation, we have focused our attention on computationally designing a Cu-hydride based *N*-heterocyclic carbene (NHC)[NHC-Cu(I)-H] that can be immobilized onto the organic linker of UiO-68 MOF. A small portion of the UiO-68 framework has been presented in Fig. 1(a). It consists of 12-connected Zr-SBU $Zr_6O_4(OH)_4$ as the MOF node and triphenyl-4,4′-dicarboxylate (TPDC) as the organic linker.[19] An enlarged view of the NHC-Cu(I)-H decorated UiO-68 MOF is presented in Fig. 1(b).

NHCs are nitrogen containing heterocyclic rings consisting of a carbene carbon. They have been extensively used to catalyse various organometallic transformations[20] and have also been used as ligands to fabricate NHC–metal complexes.[21] Coinage metal-based NHCs are widely known[22] and has been experimentally synthesised over porous framework materials.[23] Jiang *et al.* have also proposed a procedure for experimental synthesis of UiO-68 decorated with NHC-Cu(I)-H.[17] The stability of NHC-Cu(I)-H over UiO-68 was also computationally confirmed by them. We can, thus, conclude that NHC-Cu(I)-H decorated UiO-68 MOFs are feasible and hence can be realized in practice. Since (1) NHC-

Department of Chemistry, Visva-Bharati University, Santiniketan 731235, India. E-mail: pranab.sarkar@visva-bharati.ac.in

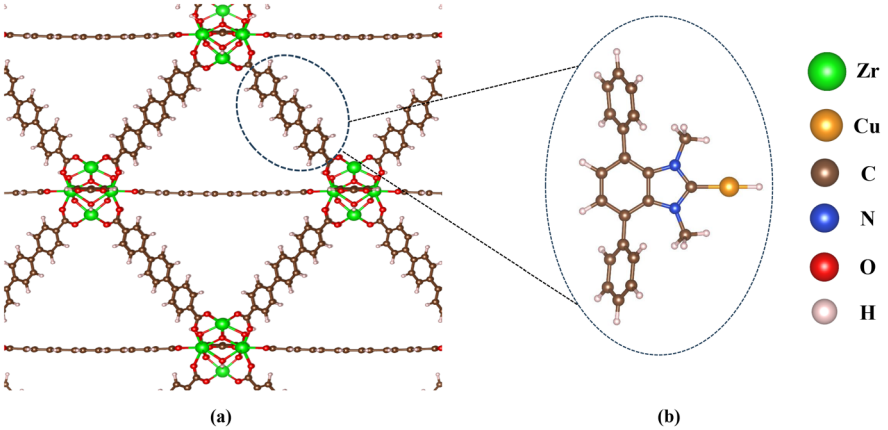

Fig. 1 (a) A small portion of the UiO-68 framework. (b) UiO-68 decorated with NHC-Cu(I)-H.

Cu(I)-H has shown to be an active catalyst for H_2 activation[24] and (2) the hydride donating ability of NHC-Cu(I)-H is high,[17] we have chosen Cu–H over the remaining coinage–metal hydrides (*i.e.* Ag–H and Au–H) for our present study.

Although Cu(I) sites have limited coordination abilities,[25] stabilization by the *N*-heterocyclic carbene ligand and the surrounding framework allows for substrate activation and reaction progression. Moreover, ethylene, carbon monoxide, and hydrogen do not bind simultaneously to the Cu(I) site; instead, they interact with the active site sequentially as the reaction progresses. Hence, ethylene hydroformylation over the Cu(I) site is expected to be feasible.

2 Computational details

In the present study, a gas-phase cluster model was used to investigate the entire catalytic pathway neglecting explicit or implicit solvation effects. This is in accordance with the experimental setting of the hydroformylation reaction, which is typically conducted under gas phase conditions. Hence, the current methodology has shown good agreement with the experimental results for MOF-based catalytic systems.[17,26–28]

Since the unit cell of UiO-68 MOF consists of a large number of atoms and we are concerned with the NHC immobilized onto the organic linker of the MOF, a 43-atom cluster model (Fig. 1b) was used to carry out Kohn–Sham density functional theory (KS-DFT) calculations using the Gaussian 16 package.[29] This cluster model has shown to be free from MOF confinement effects[17] and hence, it can be used to accurately predict catalytic properties of UiO-68 functionalized NHC-Cu(I)-H. The initial structure of the TPDC linker was obtained from the Cambridge Crystallographic Data Centre (CCDC number: 889531) onto which NHC was immobilized. This structure was optimized using the M06-L functional. The local meta-GGA M06-L functional is known to perform well for transition metals and organometallic systems while accounting for medium-range electron correlation effects.[28] Although M06-L may exhibit self-interaction error, this is not a concern here, as the valence electron configurations of the Cu(I)-centre suggests that it is a closed-shell singlet and hence involves no spin-state ambiguity. Moreover, the M06-L functional has shown good performance in reproducing experimental trends of various adsorption processes and reaction pathways over a number of MOFs.[30,31] The reactivity predicted using M06-L has shown consistency with functionals such as B3LYP-D3, PBE-D3, and M06 towards oxidative dehydrogenation of propane over NU-1000-supported heterobimetallic clusters.[27] Hence, the M06-L functional offer a practical balance between accuracy and computational efficiency. Geometry optimizations and frequency calculations were carried out using the M06-L/GENECP method with the SDD basis set and its corresponding effective core potential for Cu and def2-SVP basis set for C, H, N and O atoms. All the calculations were carried out using an ultrafine grid. The required number of imaginary frequencies was confirmed for a minima (zero) or a transition state (one and only one). Intrinsic reaction coordinate (IRC) calculations were performed to confirm that we have obtained the desired transition state. Single point energies were calculated at the M06-L/def2-TZVP level. NBO (natural bond orbital) analysis was carried out to obtain NBO charges. All reported energies are Gibbs free energies calculated at 298.15 K and 1 atm pressure.

3 Results and discussion

3.1 Features of NHC-Cu(I)-H

The optimized structure of NHC-Cu(I)-H is presented in Fig. 2. The valence electron configurations for NHC-Cu(I)-H (*i.e.* $3d^{10}$) suggest that it is a closed-shell singlet system. Calculation of the oxidation state shows that the copper centre is in the +1 oxidation state. The presence of increased electron density at the hydride species (red region in Fig. 2(a)) of NHC-Cu(I)-H confirms the strong σ-donor ability of carbene carbon. This is further confirmed by inspecting the NBO charges presented in Fig. 2(b). We, therefore, expect that the hydride species present in NHC-Cu(I)-H can be easily

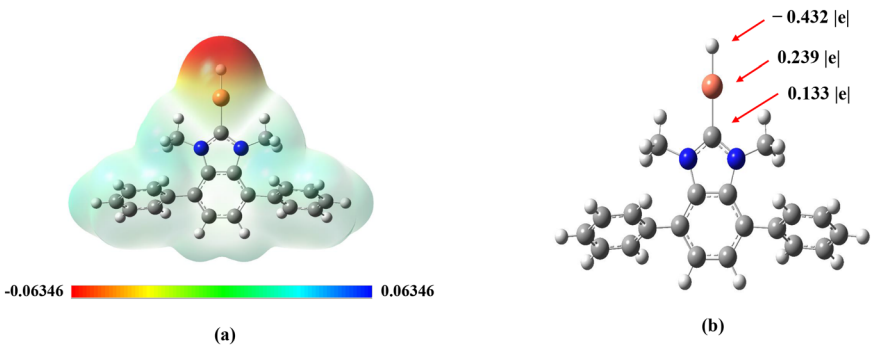

Fig. 2 (a) ESP surface map of NHC-Cu(I)-H. (b) The cluster model of NHC-Cu(I)-H showing NBO charges.

released when required to carry out the hydrogenation/hydroformylation reaction.

3.2 Catalytic pathway

Ethylene hydroformylation to propanal involves the presence of ethylene, CO and H_2 as reactants. The simultaneous presence of CO and H_2 with ethylene competes with each other for the active sites resulting in two competing pathways: (a) ethylene hydroformylation to propanal and (b) ethylene hydrogenation to ethane.

The schematic diagram for ethylene hydroformylation and ethylene hydrogenation is presented in Fig. 3. The reaction proceeds as follows:

(a) Adsorption and activation of ethylene at the Cu-centre *via* TS1. The interaction of ethylene with the Cu-centre occurs in a bridging fashion. Adsorption and activation of ethylene occurs *via* the transfer of electrons from a Cu-centred NBO with a pure *d*-character to the π^* orbital of ethylene. This has been confirmed from the second order perturbation theory analysis reporting a stabilization energy of 27.75 kcal mol^{-1} for this interaction. This is further confirmed by the reduction in the Wiberg bond index (WBI) from 2.05 (in intermediate **2**) to 1.50 (in intermediate **3**). Also, the C–C bond length has increased from 1.33 Å to 1.40 Å in moving from intermediate **2** to intermediate **3**. The activation barrier encountered during this process is 2.90 kcal mol^{-1}.

(b) Hydride transfer *via* TS2. The transfer of hydride species from the Cu-centre to an adjacent ethylene carbon results in the formation of an ethyl species (intermediate **4** [Fig. 3]). The activation barrier encountered during this process is 13.37 kcal mol^{-1}. The ethyl species now binds in a terminal mode to the Cu-centre, the WBI for which is 0.62.

It is at this point where the reaction may follow two pathways to produce different products. Interaction of CO with intermediate **4** leads to hydroformylation pathway while interaction of H_2 with intermediate **4** leads to hydrogenation pathway. Hence, CO and H_2 compete with each other for the intermediate **4**.

A close look at Fig. 4 shows that the interaction of H_2 with intermediate **4** is endergonic by 4.5 kcal mol^{-1} compared to that for CO with intermediate **4**. This indicates that CO adsorption will be favoured over H_2 adsorption.

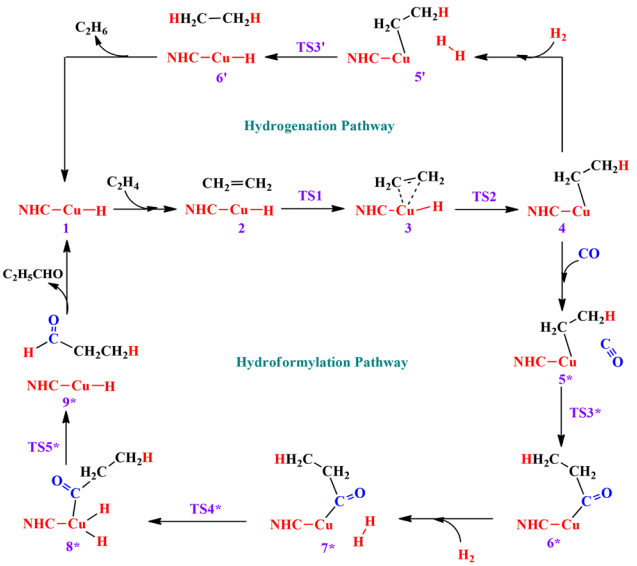

Fig. 3 Proposed mechanism of ethylene hydroformylation and ethylene hydrogenation. The resting state of the catalyst has been represented as **1** where only the Cu–H species has been shown for clarity.

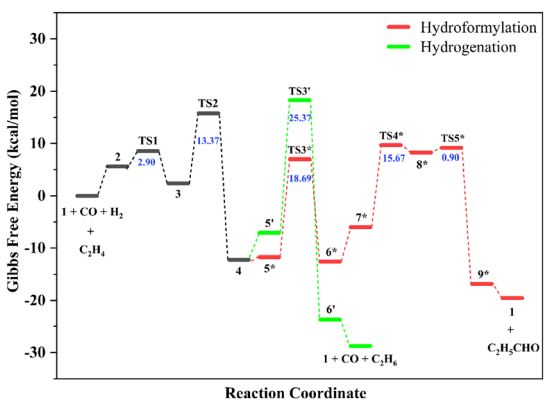

Fig. 4 Reaction profile for ethylene hydroformylation and ethylene hydrogenation. The activation barriers have been indicated in blue. All the energies have been reported relative to the separated state of the catalyst and reactants.

3.2.1 Hydroformylation to propanal

(c) Adsorption and activation of CO. Adsorption and activation of CO on the Cu-centre involves (1) transfer of non-bonding electrons situated on carbon of CO into the vacant Cu-centred NBO with a near *p*-character (stabilization energy of 219.03 kcal mol^{-1}) and (2) a back donation of electrons from the same Cu-centred NBO into the π^* orbital of CO (stabilization energy of 20.42 kcal mol^{-1}). This is further confirmed from the reduction in the WBI of CO to 2.13 in intermediate **5***.

*(d) CO insertion via **TS3**.* CO insertion into the Cu-ethyl bond occurs *via* the transfer of electron density from the ethyl carbon to the carbon of CO. The excess negative charge that builds on the carbon of CO is further neutralized by the O of CO by withdrawing electron density from carbon. This process can be understood by following the NBO charges on moving from intermediate **5*** to intermediate **6*** [Fig. 5]. This is further confirmed by the reduction in the WBI of CO to 1.79 in intermediate **6***. The activation barrier encountered during this process is 18.69 kcal mol^{-1}.

*(e) Homolytic cleavage of H_2 via **TS4**.* Adsorption of H_2 at intermediate **6*** results in intermediate **7***. That H_2 dissociates homolytically over Cu has been confirmed by following the natural electron configurations of the Cu and H atoms. Table 1 shows that each H in intermediate **8*** possess one electron each. This is in agreement with our conclusion. The activation barrier encountered during this process is 15.67 kcal mol^{-1}.

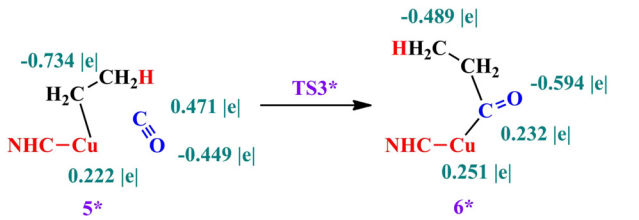

Fig. 5 The change of NBO charges on moving from intermediate **5*** to intermediate **6***. The values have been indicated in green.

*(f) Propanal formation via **TS5**.* Now, one of the dissociated H atoms gets transferred from the Cu-centre to the carbonyl carbon resulting in the formation of propanal (intermediate **9***). The activation barrier encountered during this process is as low as 0.90 kcal mol^{-1}. Desorption of propanal, at this point, (exergonic by 2.76 kcal mol^{-1}) regenerates the catalyst (intermediate **1**).

3.2.2 Hydrogenation to ethane

(c) Heterolytic dissociation of H_2. Adsorption of H_2 on intermediate **4** results in intermediate **5′**. That H_2 dissociates heterolytically over Cu has been confirmed by following the natural electron configurations of the Cu and H atoms. Table 2 shows that the electrons have been asymmetrically distributed between the two H atoms (intermediate **6′**) and hence, suggests a heterolytic cleavage. This process encounters an activation barrier of 25.37 kcal mol^{-1}. The proton resulting from this heterolytic cleavage results in the formation of ethane while regenerating the Cu(I) hydride species.

Although, the transformation from **5′** to **6′** is highly exergonic, it encounters a high activation barrier. Since thermodynamic favourability does not guarantee kinetic accessibility, the Brønsted–Evans–Polanyi (BEP) relationship is violated. However, we should remember that the BEP relationship, although a trend,[18] is not a strict rule. In this case, the high activation barrier likely reflects the energetic cost of H–H bond cleavage and hydride transfer to the Cu(I) centre, despite the high stability of the resulting product.

3.3 Homolytic *vs.* heterolytic bond cleavage

A striking difference between the hydroformylation pathway and the hydrogenation pathway is that the mode of H_2 dissociation is different in the two cases – the hydroformylation pathway involves a homolytic bond cleavage while the hydrogenation pathway encounters a heterolytic bond cleavage. A close look at the electronic environment of intermediate **7*** and **5′** reveals the reason of such difference [Fig. 6].

Table 1 Table summarizing the natural electronic configuration for the homolytic cleavage of H_2

	Natural electronic configuration
	7*
Cu	[core] 4s(0.83) 3d(9.74) 4p(0.16) 4d(0.01)
H	1s(1.06)
H	1s(0.95)
	TS4*
Cu	[core] 4s(0.55) 3d(9.64) 4p(0.82)
H	1s(1.05) 2s(0.01)
H	1s(0.98)
	8*
Cu	[core] 4s(0.59) 3d(9.59) 4p(0.83)
H	1s(1.14)
H	1s(1.04)

Table 2 Table summarizing the natural electronic configuration for the heterolytic cleavage of H_2

	Natural electronic configuration
	5′
Cu	[core] 4s(0.76) 3d(9.72) 4p(0.14)
H	1s(1.01)
H	1s(1.00)
	TS3′
Cu	[core] 4s(0.49) 3d(9.73) 4p(0.50) 4d(0.01)
H	1s(0.85)
H	1s(1.17) 2s(0.01)
	6′
Cu	[core] 4s(0.83) 3d(9.77) 4p(0.17)
H	1s(0.81)
H	1s(1.43)

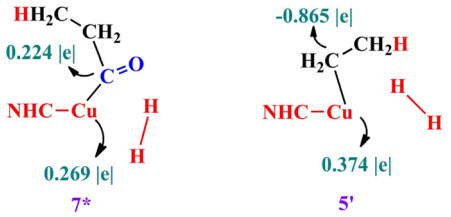

Fig. 6 The NBO charges on the Cu atom and C atom in intermediate **7*** and intermediate **5′**. The values have been indicated in green.

In case of intermediate **5′**, the Cu-centre is elecron deficient whereas the C atom of the ethyl species is highly electron dense. The electrostatic effects due to high negative charge at the C atom of the ethyl species polarize the H_2 molecule in such a way that it causes asymmetric electron distribution within the molecule. This in turn results in heterolytic cleavage of the H_2 molecule. However, in the case of intermediate **7***, the Cu-centre is less elecron deficient than that of intermediate **5′**. Moreover, the C atom of the carbonyl group is also electron deficient. This electronic environment cannot cause asymmetric polarization of the H_2 molecule and hence, homolytic bond cleavage is favoured.

3.4 Reaction selectivity

Given the two competing pathways, we would now like to get some insight into the reaction selectivity using classical transition state theory. A close look at Fig. 4 shows that the rate limiting step of the hydroformylation pathway is the CO insertion step (**TS3***) while that for the hydrogenation pathway is the heterolytic bond dissociation of H_2 (**TS3′**). Hence, the overall free energy barrier ($\Delta G^{\ddagger}_{\text{overall}}$) for both the pathways are as follows:

$$\Delta G^{\ddagger}_{\text{overall}}(\text{hydroformylation}) = 6.99 \text{ kcal mol}^{-1} \quad (1)$$

$$\Delta G^{\ddagger}_{\text{overall}}(\text{hydrogenation}) = 18.26 \text{ kcal mol}^{-1} \quad (2)$$

The rate constant of the overall reaction is 4.59×10^7 s^{-1} for the hydroformylation pathway while that of the hydrogenation pathway is 0.25 s^{-1}. This confirms that propanal formation occurs selectively over ethane formation over the UiO-68 decorated NHC-Cu(I)-H catalyst.

3.5 Comparison with previous studies

We now compare our results with the previous studies to realize its efficacy towards the ethylene hydroformylation reaction. Decker *et al.* have carried out a DFT calculation on ethylene hydroformylation using the homogeneous $HRh(PH_3)_2(CO)$ catalyst.[32] They have shown that the CO insertion step is the rate limiting step with an activation barrier of 20.4 kcal mol^{-1}. Their conclusions are in agreement with our findings. We now compare our UiO-68 decorated NHC-Cu(I)-H catalyst with other Rh-based heterogeneous catalysts.

Lee *et al.* have computationally studied ethylene hydroformylation over Rh/Al_2O_3 to investigate the influence of ReO_x promoters.[12] The activation barrier has been found to be 30.83 kcal mol^{-1} for the H_2 dissociation step in the presence of ReO_x promoters. Computational studies by Amsler *et al.* have reported the highest effective barrier of 19.36 kcal mol^{-1} while investigating the catalytic activity of Rh single atoms dispersed onto the CeO_2 surface for ethylene hydroformylation.[7] Another computational study by Huang *et al.* has investigated the promotional effect of Co on the Rh catalyst.[13] CO insertion was found to be the rate limiting step with an activation barrier of 19.6 kcal mol^{-1}.

The UiO-68 decorated NHC-Cu(I)-H is a non-Rh-based heterogeneous catalyst providing single site reactivity. Since ethylene hydroformylation using UiO-68 decorated NHC-Cu(I)-H involves an activation barrier of 18.69 kcal mol^{-1} for the CO insertion process, we can affirm that UiO-68 decorated NHC-Cu(I)-H is an efficient heterogeneous catalyst and can act as a cheap substitute for the homogeneous Wilkinson's catalyst. Moreover, it is a better alternative to various Rh-based heterogeneous systems reported above.

4 Conclusion

To sum up, in the present study, we have carried out a computational investigation on the role of a Cu-hydride based *N*-heterocyclic carbene [NHC-Cu(I)-H] immobilized onto the organic linker of UiO-68 MOF in catalysing ethylene hydroformylation reaction. Mechanistic investigation shows that NHC-Cu(I)-H, a non-Rh-based catalyst with single site reactivity, can selectively transform ethylene to propanal and can act as an alternative to the homogeneous Wilkinson's catalyst and also to various Rh-based heterogeneous catalysts. Thus, to the best of our knowledge, we have predicted for the first time a non-Rh-based catalyst for hydroformylation reaction that is both economic and efficient.

Conflicts of interest

There are no conflicts to declare.

Data availability

Supplementary information: Optimised structures of intermediates and transition states, IRC for **TS3*** and **TS3′**. See DOI: **https://doi.org/10.1039/D5CY00818B**.

The data supporting this article have been included as part of the SI.

Acknowledgements

The authors sincerely acknowledge the financial support from CSIR (HRDG), Government of India [sanction no. 01(3886)/21/EMR-II]. P. Sarkar sincerely acknowledges the financial support from UGC-BSR Mid-Career, Government of India [sanction no. F.19-257/2021(BSR)]. A. Ganai sincerely acknowledges CSIR (HRDG), Government of India for providing SRF-NET fellowship [sanction no. 09/0202 (13084)/2021-EMR-I].

Notes and references

1 R. Franke, D. Selent and A. Borner, *Chem. Rev.*, 2012, **112**, 5675–5732.
2 S. H. Chikkali, R. Bellini, B. de Bruin, J. I. van der Vlugt and J. N. Reek, *J. Am. Chem. Soc.*, 2012, **134**, 6607–6616.
3 N. Navidi, J. W. Thybaut and G. B. Marin, *Appl. Catal., A*, 2014, **469**, 357–366.
4 T. P. Clark, C. R. Landis, S. L. Freed, J. Klosin and K. A. Abboud, *J. Am. Chem. Soc.*, 2005, **127**, 5040–5042.
5 Y. Jiao, M. S. Torne, J. Gracia, J. H. Niemantsverdriet and P. W. van Leeuwen, *Catal. Sci. Technol.*, 2017, **7**, 1404–1414.
6 J. Ma, M. Liu, M. Zhu, Y. Wang, Y. Zhou and B. Wang, *Catal. Sci. Technol.*, 2022, **12**, 6740–6750.
7 J. Amsler, B. B. Sarma, G. Agostini, G. Prieto, P. N. Plessow and F. Studt, *J. Am. Chem. Soc.*, 2020, **142**, 5087–5096.
8 R. Lang, T. Li, D. Matsumura, S. Miao, Y. Ren, Y.-T. Cui, Y. Tan, B. Qiao, L. Li and A. Wang, *et al.*, *Angew. Chem., Int. Ed.*, 2016, **55**, 16054–16058.
9 L. Wang, W. Zhang, S. Wang, Z. Gao, Z. Luo, X. Wang, R. Zeng, A. Li, H. Li and M. Wang, *et al.*, *Nat. Commun.*, 2016, **7**, 14036.
10 L. Sordelli, M. Guidotti, D. Andreatta, G. Vlaic and R. Psaro, *J. Mol. Catal. A: Chem.*, 2003, **204**, 509–518.
11 B. Liu, N. Huang, Y. Wang, X. Lan and T. Wang, *ACS Catal.*, 2021, **11**, 15235–15243.
12 S. Lee, A. Patra, P. Christopher, D. G. Vlachos and S. Caratzoulas, *ACS Catal.*, 2021, **11**, 9506–9518.
13 N. Huang, B. Liu, X. Lan and T. Wang, *Ind. Eng. Chem. Res.*, 2020, **59**, 18771–18780.
14 K. Zhao, X. Wang, D. He, H. Wang, B. Qian and F. Shi, *Catal. Sci. Technol.*, 2022, **12**, 4962–4982.
15 A. Bavykina, N. Kolobov, I. S. Khan, J. A. Bau, A. Ramirez and J. Gascon, *Chem. Rev.*, 2020, **120**, 8468–8535.
16 A. Ganai and P. Sarkar, *J. Org. Chem.*, 2024, **89**, 12010–12019.
17 K. Yang and J. Jiang, *ACS Appl. Mater. Interfaces*, 2021, **13**, 58723–58736.
18 A. Ganai, B. Ball and P. Sarkar, *J. Phys. Chem. Lett.*, 2023, **14**, 1832–1839.
19 X. Ye and D. Liu, *Cryst. Growth Des.*, 2021, **21**, 4780–4804.
20 D. M. Flanigan, F. Romanov-Michailidis, N. A. White and T. Rovis, *Chem. Rev.*, 2015, **115**, 9307–9387.
21 T. Scattolin and S. P. Nolan, *Trends Chem.*, 2020, **2**, 721–736.
22 J. C. Lin, R. T. Huang, C. S. Lee, A. Bhattacharyya, W. S. Hwang and I. J. Lin, *Chem. Rev.*, 2009, **109**, 3561–3598.
23 Y. Li, Y. Dong, J.-L. Kan, X. Wu and Y.-B. Dong, *Org. Lett.*, 2020, **22**, 7363–7368.
24 N. Rui, F. Zhang, K. Sun, Z. Liu, W. Xu, E. Stavitski, S. D. Senanayake, J. A. Rodriguez and C.-J. Liu, *ACS Catal.*, 2020, **10**, 11307–11317.
25 J. T. Rubino and K. J. Franz, *J. Inorg. Biochem.*, 2012, **107**, 129–143.
26 M. Barona, S. Ahn, W. Morris, W. Hoover, J. M. Notestein, O. K. Farha and R. Q. Snurr, *ACS Catal.*, 2019, **10**, 1460–1469.
27 M. C. Simons, M. A. Ortuño, V. Bernales, C. A. Gaggioli, C. J. Cramer, A. Bhan and L. Gagliardi, *ACS Catal.*, 2018, **8**, 2864–2869.
28 D. R. Pahls, M. A. Ortuno, P. H. Winegar, C. J. Cramer and L. Gagliardi, *Inorg. Chem.*, 2017, **56**, 8739–8743.
29 M. J. Frisch, G. W. Trucks, H. B. Schlegel, G. E. Scuseria, M. A. Robb, J. R. Cheeseman, G. Scalmani, V. Barone, G. A. Petersson, H. Nakatsuji, X. Li, M. Caricato, A. V. Marenich, J. Bloino, B. G. Janesko, R. Gomperts, B. Mennucci, H. P. Hratchian, J. V. Ortiz, A. F. Izmaylov, J. L. Sonnenberg, D. Williams-Young, F. Ding, F. Lipparini, F. Egidi, J. Goings, B. Peng, A. Petrone, T. Henderson, D. Ranasinghe, V. G. Zakrzewski, J. Gao, N. Rega, G. Zheng, W. Liang, M. Hada, M. Ehara, K. Toyota, R. Fukuda, J. Hasegawa, M. Ishida, T. Nakajima, Y. Honda, O. Kitao, H. Nakai, T. Vreven, K. Throssell, J. A. Montgomery Jr., J. E. Peralta, F. Ogliaro, M. J. Bearpark, J. J. Heyd, E. N. Brothers, K. N. Kudin, V. N. Staroverov, T. A. Keith, R. Kobayashi, J. Normand, K. Raghavachari, A. P. Rendell, J. C. Burant, S. S. Iyengar, J. Tomasi, M. Cossi, J. M. Millam, M. Klene, C. Adamo, R. Cammi, J. W. Ochterski, R. L. Martin, K. Morokuma, O. Farkas, J. B. Foresman and D. J. Fox, *Gaussian~16 Revision C.01*, 2016.
30 P. Verma, X. Xu and D. G. Truhlar, *J. Phys. Chem. C*, 2013, **117**, 12648–12660.
31 V. Bernales, A. B. League, Z. Li, N. M. Schweitzer, A. W. Peters, R. K. Carlson, J. T. Hupp, C. J. Cramer, O. K. Farha and L. Gagliardi, *J. Phys. Chem. C*, 2016, **120**, 23576–23583.
32 S. A. Decker and T. R. Cundari, *Organomet.*, 2001, **20**, 2827–2841.